

Excitonic fine structure of epitaxial Cd(Se,Te) on ZnTe type-II quantum dots

Petr Klenovský^{1,2,*}, Piotr Baranowski^{3,†} and Piotr Wojnar^{3,‡}

¹Department of Condensed Matter Physics, Faculty of Science, Masaryk University, Kotlářská 267/2, 61137 Brno, Czech Republic

²Czech Metrology Institute, Okružní 31, 63800 Brno, Czech Republic

³Institute of Physics, Polish Academy of Sciences, Al Lotników 32/46, PL-02-668 Warsaw, Poland



(Received 13 December 2021; revised 31 March 2022; accepted 4 April 2022; published 2 May 2022)

The structure of the ground-state exciton of Cd(Se,Te) quantum dots embedded in ZnTe matrix is studied experimentally using photoluminescence spectroscopy and theoretically using $\mathbf{k} \cdot \mathbf{p}$ and configuration interaction methods. The experiments reveal a considerable reduction of fine-structure splitting energy of the exciton with an increase of Se content in the dots. That effect is interpreted by theoretical calculations to originate due to the transition from spatially direct (type-I) to indirect (type-II) transition between electrons and holes in the dot induced by an increase of Se. The trends predicted by the theory match those of the experimental results very well. The theory identifies that the main mechanism causing elevated fine-structure energy, in particular in type-I dots, is due to the multipole expansion of the exchange interaction. Moreover, the theory reveals that for Se contents in the dot >0.3 , there also exists a peculiar type of confinement showing signatures of both type I and type II and which exhibits extraordinary properties, such as an almost purely light hole character of exciton and toroidal shapes of hole states.

DOI: [10.1103/PhysRevB.105.195403](https://doi.org/10.1103/PhysRevB.105.195403)

I. INTRODUCTION

Key components of future quantum devices for usage in information technology will be on-demand sources of single photons and entangled photon pairs. A prominent candidate systems in this respect are currently the quantum dots (QDs). Mainly semiconductor type-I QDs where both electron and hole wave functions are bound inside the QD body show excellent optical properties combined with their compatibility with current semiconductor processing technology and, moreover, they offer the potential for scalability [1–8]. QDs currently cover a rather wide range of topics, from quantum cryptography protocols [9,10], sources of polarization-entangled photon pairs [11–13], quantum key distribution [14,15], quantum gates [16–20], or as nanomemories [18,21–26].

One of the key challenges for turning QDs into sources of entangled photons is to zero the tiny energy separation of the bright doublet of the ground-state exciton (X^0), dubbed the fine-structure splitting (FSS). That can be achieved, e.g., by externally applying elastic strain [27–32], electric [13], or magnetic [33–35] fields. A further option to have QDs

with negligible FSS is provided by growing QDs on lattice-matched materials [36,37].

Another route of obtaining small FSS is utilizing type-II QDs where one of the quasiparticles, electron or hole, is bound outside of the QD body while the other resides inside [7,38–43]. The aforementioned type-II QDs were mostly realized on group III–V materials, InAs, GaAs, and GaSb. However, there exists another class of type-II QD structures based on II–VI materials like the Cd(Se,Te)/ZnTe dots. Note, however, that our purpose in this work is not to study the feasibility of Cd(Se,Te)/ZnTe dots for the generation of entangled photons but rather to study the reduction of FSS with increased electron-hole spatial separation.

CdSe/ZnTe is a semiconductor system, which is well known for its type-II band alignment in which the spatially indirect optical emission appears in the near infrared spectral region, i.e., at 1.0–1.1 eV. This fact has been demonstrated experimentally in CdSe/ZnTe quantum wells [44], CdSe/ZnTe core/shell nanowires [45], and colloidal core/shell nanocrystals [46]. However, the lattice mismatch which is the driving force for the formation of self-assembled QDs is very small and amounts to 0.003 in this material system, which prevents the formation of type-II CdSe/ZnTe QDs.

On the other hand, a sufficiently large lattice mismatch of 0.07 is present in the CdTe/ZnTe semiconductor system which has enabled the growth of CdTe/ZnTe QDs by molecular beam epitaxy [47,48]. Subsequently, their optical properties have been the subject of extensive investigations [49–51]. In particular, it was found that this semiconductor system is characterized by the type-I confinement which is manifested by quite short excitonic lifetimes, i.e., below 500 ps [52]. However, the valence band offset in these structures is quite small [53] whereas only strain effects are responsible for its type-I character. That is why the addition of a certain

*klenovsky@physics.muni.cz.

†baranowski@ifpan.edu.pl.

‡wojnar@ifpan.edu.pl.

amount of selenium into Cd(Se,Te) QD-layer, leading to the shift of the valence band toward lower energies, results in the transition from type-I to type-II confinement [54]. At the same time the Cd(Se,Te)/ZnTe lattice mismatch is sufficiently large to induce the QD formation and the optical emission from these structures is intense enough to enable the observation of the emission from individual QDs, which enables the unique study of FSS in those type-II QDs that we discuss in this work.

The paper is organized as follows. We start with a description of the experiments, i.e., the growth of Cd(Se,Te)/ZnTe QDs and measurements of their optical emission, revealing FSS of that system as a function of Se content. That is followed by theory discussion of the electronic structure of Cd(Se,Te)/ZnTe QDs, starting from analysis of the single-particle (SP) states and carrying on to computations of correlated excitons, finally showing that the trends predicted by theory match those of the experimental results very well. Furthermore, the theory shows a rather unusual behavior of Cd(Se,Te)/ZnTe QDs related to light hole (LH) exciton and the Aharonov-Bohm effect. We note that since we were mainly interested in whether or not the trends observed in the experiment are seen also in theory, we did not focus on tuning of material parameters in our calculation or dot shapes and dimensions in that. The latter was directly taken from the experiment and Ref. [54].

II. EXPERIMENT

The samples containing self-assembled Cd(Se,Te)/ZnTe QDs are grown by the molecular beam epitaxy. The details of the growth procedure are described in Ref. [54]. The optically active part of the samples consists of a layer of Cd(Se,Te) QDs embedded in the ZnTe matrix. Three samples with a different average Se concentrations within the dots equal to 0.002, 0.03, and 0.1 are investigated for the purposes of the present work. Se content within QDs can be effectively changed by varying the growth parameters during the deposition of the QD layer. That layer consists, consecutively, of three CdTe monolayers, one CdSe submonolayer, and two CdTe monolayers. Depending on the coverage of the central CdSe monolayer, which is controlled by the exposure time of Se flux, the average Se concentration can be varied from 0 up to 0.17. The largest Se concentration corresponds to the deposition of a complete central CdSe monolayer. After the deposition of the QD layer, the QD-formation process does not take place spontaneously despite the large lattice mismatch, as is common for a II–VI semiconductor system. It has to be additionally induced by tellurium deposition at low substrate temperature and its subsequent thermal desorption [47,48]. In the final step, the dots are capped with a 50 nm-thick ZnTe layer.

Photoluminescence (PL) measurements performed at low temperature reveal that the emission energy strongly depends on Se concentration within the Cd(Se,Te) QDs which is induced, most likely, by the change of confinement from type-I to type-II [54]. In particular, it is found that the maximum emission energy amounts to 1.98, 1.83, and 1.69 eV for the investigated mean Se concentrations of 0.002, 0.03, and 0.1,

respectively. This choice of the samples along with the inhomogeneous broadening of the emission bands, which amounts typically to 80 meV, ensures that the emission lines from individual QDs can be found in the entire spectral range, from 1.5 up to 1.9 eV.

In order to assess the emission from individual QDs, μ -PL measurements in which the excitation laser spot is reduced to 3 μ m are performed. Further reduction of the excitation area is obtained using apertures with a diameter of 400 nm within a 150 nm-thick gold layer deposited on top of the structures. For the measurements, the samples are placed inside a continuous flow cryostat in which the temperature is kept at 7 K.

Several emission lines with the spectral width in the range of 500 μ eV – 1 meV originating from individual QDs are observed. In order to determine the corresponding excitonic FSS values, linear polarization of the optical emission spectrum has been measured. This study is performed in geometry in which light propagates perpendicular to the sample surface and the linear polarization vector is always parallel to the sample plane. It is found that the emission energy slightly depends on the linear polarization angle for all measured bands. In Fig. 1(a), the emission lines are measured in two orthogonal linear polarizations corresponding to the largest change of the emission energy. In such configuration, the energy difference is given by the value of FSS. In order to determine the best FSS values, the spectral position is plotted as a function of the polarization angle for both emission lines; see Fig. 1(b). It is found that this dependence can be well fitted with a sine square function, whereas its amplitude gives us directly the FSS value [49,55]. FSS values of the two emission bands presented in Figs. 1(a) and 1(b) are found to be very similar. However, both polarization angle dependencies are shifted by 90° with respect to each other; see Fig. 1(b). This feature is characteristic for biexciton and single exciton emissions and indicates that both bands originate from the same QD. In order to identify whether the particular band corresponds to the single exciton or to the biexciton emission, excitation power dependence of the optical emission spectrum has been measured; see inset in Fig. 1(a). The intensity of the high-energy line at 1.798 eV increases almost linearly with increasing excitation power whereas the intensity of the low-energy line at 1.796 eV increases superlinearly, which leads us to associate them to the single exciton and biexciton emissions, respectively.

In Fig. 1(c), FSS values from over 40 individual QDs are plotted as a function of the single exciton emission energy. A large distribution of FSS values decreasing from \sim 300 μ eV to almost zero is found among the investigated dots. Most importantly, they depend conspicuously on the exciton emission energy. Significantly, smaller FSS values are observed, on average, for the dots emitting at lower energies compared with the dots emitting at higher energies. The large variation of these values at a fixed energy results, most likely, from the anisotropy of the potential localizing charge carriers which is induced by the shape and/or strain anisotropy of the dots similar to CdTe/ZnTe QDs without Se [50]. On the other hand, the maximum emission energy depends primarily on the Se concentration within the dots [54]. At the same time, it is found that the sizes and shapes of the dots do not change significantly as a function of Se content within the investigated

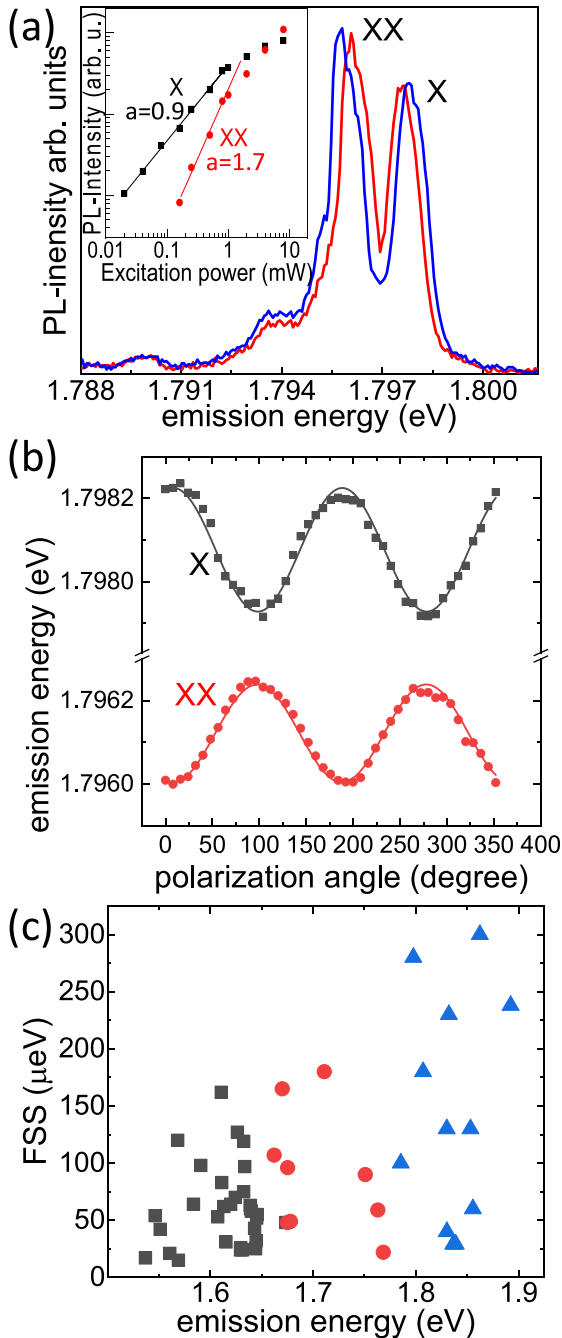


FIG. 1. Fine FSS of individual Cd(Se,Te)/ZnTe QDs for (a) exciton (X) and biexciton (XX) emission from a single Cd(Se,Te)/ZnTe QD measured in two orthogonal linear polarizations corresponding to the anisotropy axes of the dot (b) spectral position of the exciton and biexciton emission from the same dot as a function of the polarization angle. Solid lines represent fits with sine square functions from which the FSS value of $275 \mu\text{eV}$ is determined. (c) FSS values for various individual QDs as a function of the exciton emission energy. The inset of panel (a) shows the measured (points) and fitted (lines) dependencies of X (black) and XX (red) with slopes $a = 0.9$ and $a = 1.7$, respectively. The dots are taken from three samples with different average Se concentrations of 0.002, 0.03, and 0.1 which are marked in (c) with different colors: Blue, red, and dark gray, respectively. Temperature during these measurements was kept at 7 K, the excitation laser wavelength was 405 nm, and the laser spot diameter was $\sim 3 \mu\text{m}$.

concentration range as demonstrated previously by atomic force microscopy [54]. Thus, it is reasonable to conclude that the increase of the average Se concentration within Cd(Se,Te) QDs leads to the overall decrease of FSS values. A possible explanation of this effect relies on the change of the confinement of the dot/matrix interface character from type-I to type-II, leading to the increase of electron-hole spatial separation. Furthermore, the effect of mutual compensation of electron and hole wave-function anisotropies may result in the observed decrease of FSS values in type-II QDs, as predicted theoretically in Ref. [56].

Based on the growth procedure and the optical measurements presented above, we cannot draw any definite conclusion about the Se composition profile within the dots. In our considerations a uniform Se distribution is assumed for simplicity. In fact, the presence of Se- and Te-rich regions within the dot inducing additional electron-hole separation within the dots cannot be excluded. Such effects have already been studied in entirely type-I QD systems in which Cd(Se,Te) were embedded into a ZnSe matrix [57]. One of the conclusions of that work was that the FSS values were even slightly increased in the presence of Se atoms as compared with pure CdSe/ZnSe QDs and CdTe/ZnTe QDs. Since in the presently described Cd(Se,Te)/ZnTe QDs a decrease of the average FSS values takes place with an increasing Se-content, we do not expect that the local variation of Se and Te within the dots significantly impacts our results.

The most distinct experimental trends concerning the optical emission from Cd(Se,Te)/ZnTe QDs, which appear as a function of increasing Se concentration within the dots, are presented in Fig. 2. First of all, a considerable redshift of the emission energy from 1.98 eV down to 1.6 eV is observed; see Fig. 2(a). That is accompanied by a decrease of the decay rate by one order of magnitude; see Fig. 2(b). Since the PL decays can be well described by biexponential functions [54] for all samples, the fast and slow decay rates are determined and plotted in blue and red in Fig. 2(b), respectively. Finally, those results are compared with the dependence of FSS values as a function of Se concentration, which are the main subject of this work; see Fig. 2(c). The values presented in Fig. 2(c) are obtained from the arithmetic average from all QD excitons observed on a given sample. The three experimental points correspond to the three samples with different average Se concentrations investigated in this work. Despite the fact that there is a large distribution of FSS values, a clear decrease of average FSS values with increasing Se concentration is observed. In the case of Cd(Se,Te)/ZnTe QDs with a Se content of 0.17, the optical emission was too weak to perform a detailed FSS investigation like in the other samples with lower Se content.

Note that the distinct decrease of the decay rates strongly indicates the type-II character of the QDs and is caused directly by the electron-hole wave-function spatial separation. The huge emission energy redshift of 350 meV is also consistent with the type-II confinement in CdSeTe/ZnTe QDs with relatively large Se content. A Cd(Se,Te) band-gap reduction cannot explain this effect since it is expected to amount to only 135 meV at maximum (for a Se concentration of 0.4) due to the bowing effect [58].

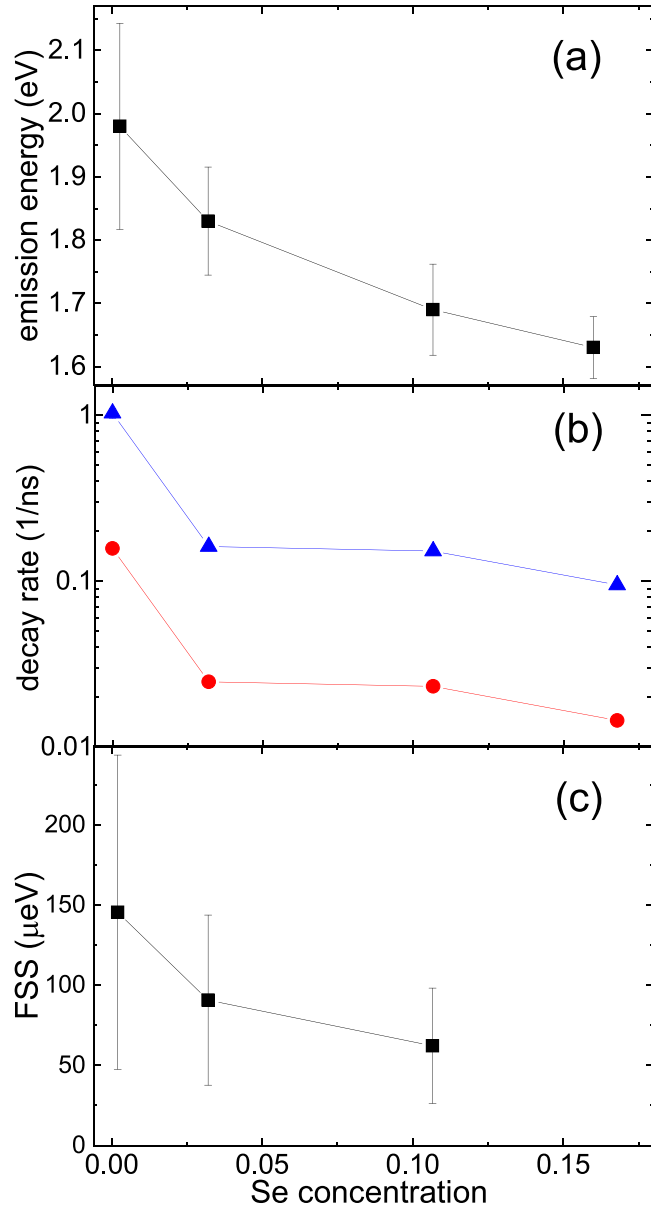


FIG. 2. Dependence of selected optical properties on the Se concentration within Cd(Se,Te)/ZnTe QDs (a) emission energy; (b) decay rates, whereas fast and slow decay are shown in blue and red, respectively; (c) average FSS determined from the data presented in Fig. 1(c). The temperature of the measurements was 7 K and the excitation laser wavelength was 405 nm. Note that the linear interpolation between data points is only for a guide of the eye.

III. THEORY

Based on the aforementioned experimental results, we will now provide the theoretical reason for the reduction of FSS values with increasing Se content. In order to do so, we calculate the correlated electronic structure of the ground-state exciton (X^0) using a combination of the eight-band $\mathbf{k} \cdot \mathbf{p}$ method [59–61], providing SP basis states for the configuration interaction (CI) [62] algorithm which we developed earlier; see Ref. [43]. During the CI calculation our CI code also evaluates the emission radiative rate [18,43] utilizing the Fermi's golden rule [63].

More specifically, we consider [35,43,61] the SP states as a linear combination of s orbital-like and x, y, z p orbital-like Bloch waves at the Γ point of the Brillouin zone, i.e.,

$$\Psi_{a_i}(\mathbf{r}) = \sum_{v \in \{s, x, y, z\} \otimes \{\uparrow, \downarrow\}} \chi_{a_i, v}(\mathbf{r}) u_v^\Gamma. \quad (1)$$

Here u_v^Γ is the Bloch wave function of an s -like (CB) or a p -like valence band at the Γ point, \uparrow/\downarrow mark the spin, and $\chi_{a_i, v}$ is the envelope function for $a_i \in \{e_i, h_i\}$.

On the other hand, in CI we consider the excitonic wave function as a linear combination of the Slater determinants (SDs),

$$\psi_i^X(\mathbf{r}) = \sum_{m=1}^{n_{\text{SD}}} \eta_{i, m} D_m^X(\mathbf{r}), \quad (2)$$

where n_{SD} is the number of SDs $D_m^X(\mathbf{r})$, and $\eta_{i, m}$ is the i -th CI coefficient which is found along with the eigenenergy using the variational method by solving the Schrödinger equation

$$\hat{H}^X \psi_i^X(\mathbf{r}) = E_i^X \psi_i^X(\mathbf{r}), \quad (3)$$

where E_i^X is the i -th eigenenergy of excitonic state $\psi_i^X(\mathbf{r})$, and \hat{H}^X is the CI Hamiltonian which reads

$$\hat{H}^X = \hat{H}_0^{\text{SP}} + \hat{V}^X, \quad (4)$$

where \hat{H}_0^{SP} and \hat{V}^X represent the Hamiltonian of the noninteracting SP states and the Coulomb interaction between them, respectively. The matrix element of \hat{V}^X is [18,35,43]

$$\begin{aligned} \langle D_n^X | \hat{V}^X | D_m^X \rangle = & -\frac{1}{4\pi\epsilon_0} \sum_{ijkl} \iint d\mathbf{r} d\mathbf{r}' \frac{e^2}{\epsilon(\mathbf{r}, \mathbf{r}') |\mathbf{r} - \mathbf{r}'|} \\ & \times \{ \Psi_i^*(\mathbf{r}) \Psi_j^*(\mathbf{r}') \Psi_k(\mathbf{r}) \Psi_l(\mathbf{r}') \\ & - \Psi_i^*(\mathbf{r}) \Psi_j^*(\mathbf{r}') \Psi_l(\mathbf{r}) \Psi_k(\mathbf{r}') \}, \end{aligned} \quad (5)$$

where e labels the elementary charge and $\epsilon(\mathbf{r}, \mathbf{r}')$ is the spatially dependent dielectric function. Note that the minus sign in front of the integral in Eq. (5) results from a different sign of the charge of the electron and hole from which exciton is composed. The sixfold integral in Eq. (5) is evaluated using the Green's function method [35,43,62,64]. Note that for $\epsilon(\mathbf{r}, \mathbf{r}')$ in Eq. (5) we use the positionally dependent bulk dielectric constant in our CI calculations. Further, the multipole expansion of the exchange interaction is included in our CI for CI basis consisting of two electron and two hole SP ground states following the theory outlined in Refs. [56] and [65].

IV. RESULTS AND DISCUSSIONS

The electronic states of Cd(Se,Te)/ZnTe QDs computed using the aforementioned $\mathbf{k} \cdot \mathbf{p}$ +CI method are shown in Fig. 3. Motivated by typical structure pinpointed in Ref. [54], the computed shape of the Cd(Se,Te) QD was a truncated cone with lower and upper basis diameters of 36 and 22 nm, respectively, and with a height of 4 nm. Except for the QD body, the rest of the simulation space consisted of ZnTe. After definition of the structure, the elastic strain tensor was obtained in the whole simulated structure by grid-pointwise minimization of elastic energy. Thereafter, the Coulomb potential energy, including the effects of the piezoelectricity, was obtained by

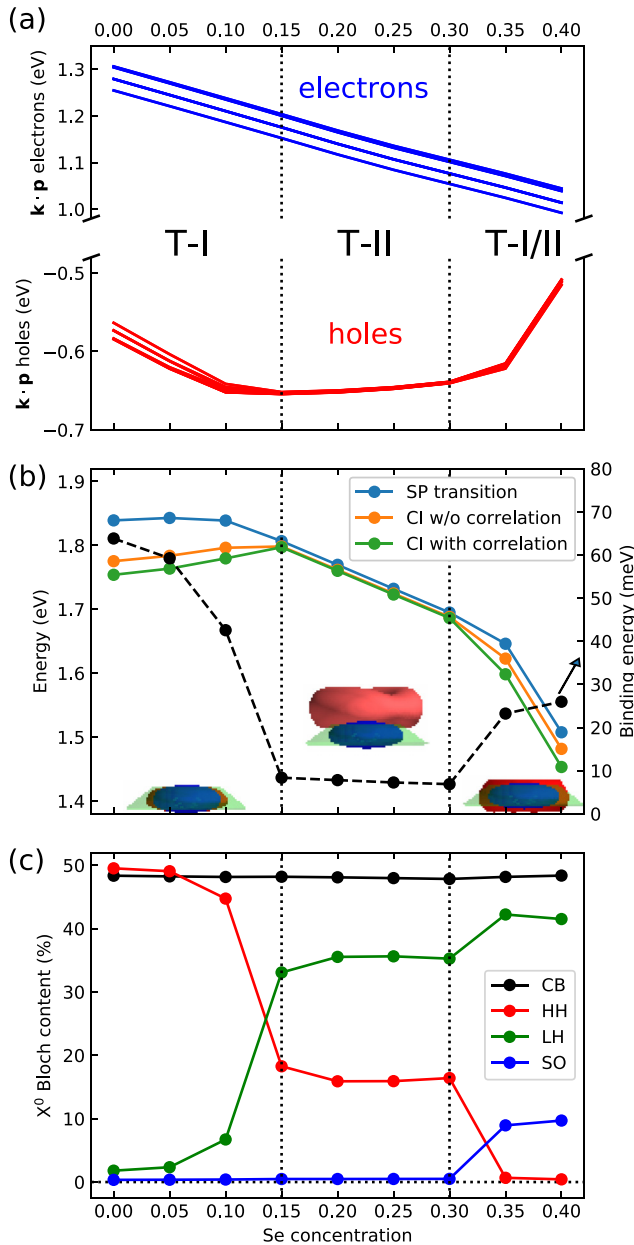


FIG. 3. Electronic states of Cd(Se,Te)/ZnTe QDs. In panel (a) we show 12 SP energies of electrons (blue) and holes (red). The inset in (a) gives markings of different types of confinement in Cd(Se, Te)/ZnTe QDs, i.e., type I (mark T-I) for Se = 0–0.15, type II (mark T-II) for Se = 0.15–0.3, and a type I/II (mark T-I/II) for Se = 0.3–0.4. In (b) we show the SP energies (blue curve) and that computed using CI without (orange curve) and with (green curve) the inclusion of the effect of Coulomb correlation. In (b) we also give the binding energy of X^0 with respect to the SP transition (black broken curve) with the energy axis on the right. The insets in (b) show side cuts of our QD (green object) and the SP electron (blue object) and hole (red object) probability densities. Panel (c) gives the conduction (CB, black), heavy-hole (HH, red), light-hole (LH, green), and spin-orbit split off (SO, blue) Bloch band content of X^0 as a function of Se concentration computed [35] using CI with 12 electron and 12 hole SP basis states, i.e., including the effect of correlation. The transitions between different confinements are marked in all panels by black dotted vertical lines. Note that the linear interpolation between data points is only for a guide of the eye.

solving the Poisson’s equation in the whole structure. The resulting Hamiltonian matrix was then diagonalized using the Nextnano++ [59,60] simulation tool, which was also used for the aforementioned computation steps. Note that all the material parameters including the effective masses were taken from the library of the Nextnano++ software [59].

The resulting eigenenergies and eigenfunctions are shown in Fig. 3(a) and Fig. 4, respectively, for 12 electron and 12 hole SP states. Depending on the Se content, we have identified three types of confinement in our QDs, i.e., type I for Se = 0–0.15, type II for Se = 0.15–0.3, and so-called type I/II for Se = 0.3–0.4. Note that the type-II confinement was identified by the spatial location of hole wave functions [inset in Fig. 3(b) and Fig. 4(b)] being outside of the QD body, while electrons are firmly bound inside the QD for all Se contents. The type I/II confinement is peculiar and shows features of the remaining two types of confinement. While the energy of electron SP states reduces with a similar rate for all Se contents, including that for SP excited states, the holes are affected by Se content and the associated type of confinement considerably more. While for type I and associated Se contents <0.15, hole SP energy decreases (i.e., the absolute value of hole energy increases), for type II it increases only slightly and, finally, for type I/II the increase of hole SP energy (decrease of the absolute value of that) with increasing Se content is observed.

As a result of the aforementioned discussion, the SP electron-hole transition energy [see blue curve in Fig. 3(b)] remains almost constant for increasing Se content in type I, while its magnitude is reduced with an increase of Se for type II and type I/II.

The Se content-dependent energies of X^0 computed by CI without and with considering the effect of correlation are shown by orange and green curves, respectively, in Fig. 3(b). Note that by the “effect of correlation” we mean specifically the expansion of CI complexes into the basis consisting not only from ground but also from excited SP states. Now the binding energy of X^0 [Fig. 3(b)] compared with electron-hole transition SP energy decreases in type I from 70 meV for Se content of zero to 10 meV for content of 0.15. The large binding energies in type I are due to the attractive Coulomb interaction between tightly quantum confined electrons and holes in QD [66]. For Se content between 0.15 and 0.3 (type II), the binding energy remains constant at 10 meV and further increases with Se content to 30 meV in type I/II. The correlation further increases the binding energy by 20 meV for Se content of zero up to by almost 30 meV for Se content of 0.4. In type II the additional binding energy due to correlation is ~ 2 meV. Finally, note that the magnitude of the reduction of X^0 energy with increasing Se content matches that observed from the spectral shift of the maximum of PL spectra in Ref. [54]. We note, however, that there is a certain discrepancy between the absolute values of simulated and measured emission energies which is mainly due to the choice of QD dimensions and shape used for the calculations.

In Fig. 3(c) we show the Se-dependent Bloch state content of X^0 , obtained from the Bloch state composition of electron and hole SP states, utilizing the squares of CI wave-function coefficients $\eta_{i,m}$ from Eq. (2). The method was previously developed in Refs. [13] and [35]. Note that the studied Bloch

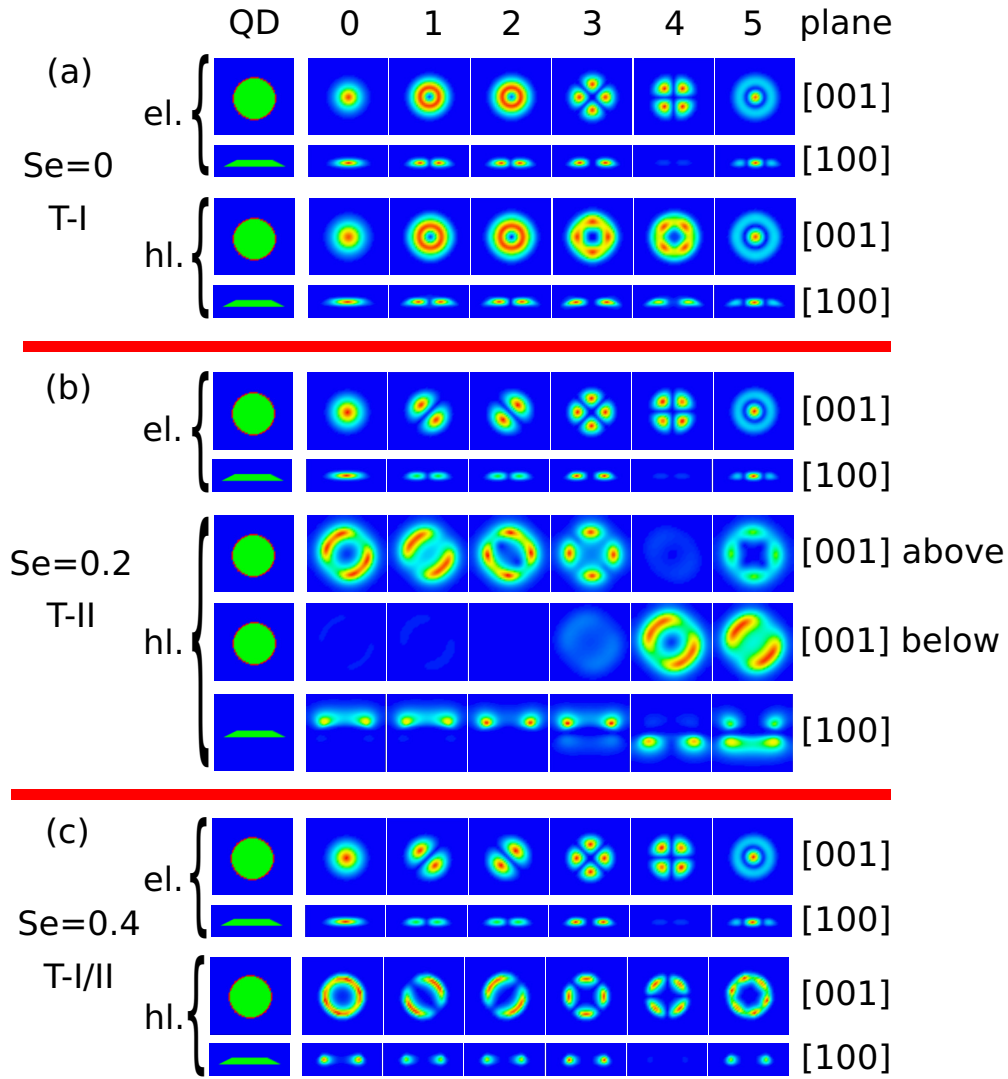


FIG. 4. Cuts of the SP probability densities of Cd(Se,Te)/ZnTe QDs for (a) zero Se content, (b) Se content of 0.2 and (c) Se content of 0.4 corresponding to type-I, type-II, and type-I/II confinement, respectively. The letters QD in the top row mark that the first column showing the cuts of the simulated QD body, and the numbers in the first row enumerate SP states starting from the ground state marked by zero. The last column gives the Miller indices of the planes where the cut was performed in each row of the figure. The abbreviations “el.” and “hl.” mark the electrons and holes, respectively. In (b) the designations “[001] above” and “[001] below” identify that the cuts of the hole densities were performed above and below the QD body, respectively, and correspond to the side cut given in the last row of panel (b).

state composition in this work is that of the CB, heavy-hole (HH), light-hole (LH, and spin-orbit (SO) valence bands.

The content of CB in X^0 is $\sim 50\%$ for all studied Se contents. While HH content is also $\sim 50\%$ for smaller Se concentrations, the increase of the amount of Se causes considerable progressive admixing of LH states in X^0 , reaching values of $\sim 40\%$ for Se contents > 0.35 . At the same time, we observe an increase of admixing of SO state for Se contents > 0.3 , reaching values as high as $\sim 10\%$. We note that for Se < 0.3 the SO content of X^0 is negligibly small.

Thus both the type-II regime and in particular the type-I/II regime show unusual composition of X^0 . Strikingly, in type I/II X^0 has an almost LH-like character with a small addition of SO states and negligible HH content. Such LH X^0 would be advantageous in quantum information technology, such as, e.g., enabling coherent conversion of photons into electron

spins [67], and was first experimentally reported in Ref. [68] for a GaAs/AlGaAs QD system where the LH character was obtained by externally applied tensile strain. However, we predict that in Cd(Se,Te)/ZnTe QDs such an LH exciton is present for Se contents > 0.35 without the necessity of any external tuning.

We now turn our attention to the theory analysis of the fine structure of X^0 and show the results in Fig. 5. We computed the fine structure employing three levels of approximation in CI, i.e., (i) without considering the effect of correlation and with the monopole-monopole term of the exchange interaction only, (ii) with correlation and the monopole-monopole term of exchange, and (iii) without correlation but with assuming the monopole-monopole, monopole-dipole, and dipole-dipole terms of the exchange interaction, what we call multipole expansion [56,69].

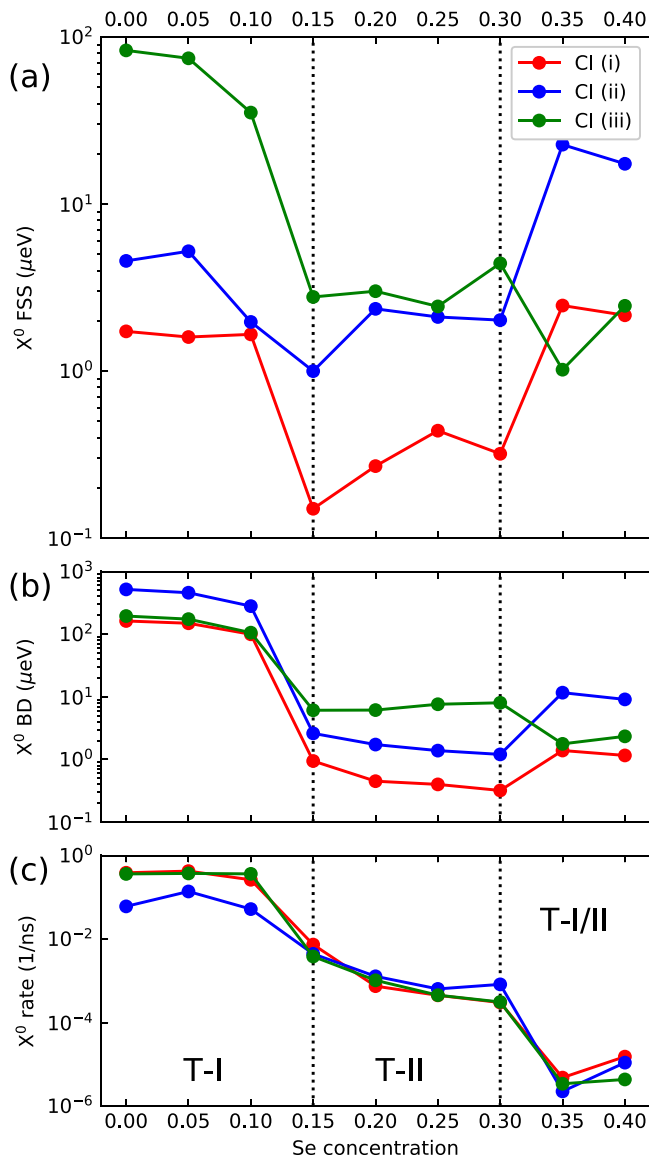


FIG. 5. Fine energy structure of ground-state exciton (X^0) in Cd(Se,Te)/ZnTe QDs as a function of Se content. In (a) we show the theory values of FSS obtained using CI with different levels of approximation, i.e., without including the effect of correlation as well as without considering the multipole expansion of exchange interaction (“CI (i),” red curve), that for data with correlation included and without multipole (“CI (ii),” blue curve), and without the effect of correlation but with multipole expansion included (“CI (iii),” green curve). Panel (b) shows the calculated values of energy splitting between bright and dark excitons (X^0 BD) and in (c) we give the computed values of the corresponding X^0 emission rates. Note that the colors of the theory curves in (b) and (c) correspond to the same CI approximations as was described for (a). The transitions between different confinements are marked in all panels by black dotted vertical lines. Note that the linear interpolation between data points is only for a guide of the eye. We further note that the cusp and diplike behavior in (a) and (c) in particular around Se contents of 0.15 and 0.3 is due to the numerical errors in our computations, see also the main text, visually magnified by the logarithmic scale used on the vertical axis.

The results for FSS of X^0 are given in Fig. 5(a) by circles and full curves. First, we see that FSS values computed using approximations (i) and (ii) defined in previous paragraph are $<10 \mu\text{eV}$ for all studied Se concentrations. However, the multipole expansion of exchange, i.e., point (iii) above, gives more realistic estimation of FSS, when compared with experimental data (Figs. 1 and 2), in particular for type-I confinement. Furthermore, we find that the reduction of FSS when going from type I to type II confinement in our system is associated with the decrease of the magnitude of multipole expansion of the exchange interaction, predominantly the dipole-dipole term [56,66]. Similarly, for the transition between type II and type I/II, the FSS is increased again up to $20 \mu\text{eV}$ which is associated with the increased importance of the effect of the Coulomb correlation.

In Fig. 5(b) we show the energy difference between optically active (bright) and inactive (dark) X^0 doublets and we mark that as X^0 BD in that panel. We see that similarly to FSS, X^0 BD is larger in type-I regime. Interestingly, contrary to FSS, BD is dominated in type I by the approximation (ii), i.e., the correlation, which causes FSS to be more than twice larger than that found by approximations (i) and (iii). On the other hand, in type II, BD is caused predominantly by approximation (iii), i.e., multipole expansion. Finally, BD for type I/II is again caused mainly by correlation [approximation (ii)].

Furthermore, we see the theory prediction of X^0 radiative rate computed by our $\mathbf{k} \cdot \mathbf{p}$ +CI computational complex in Fig. 5(c). We observe that the computed rates for all three approximations (full curves) are close to the experimental results in Fig. 2(b). As expected, the emission rate of our dots in type II ($\sim 10^{-3}$ 1/ns) is reduced by two orders of magnitude compared with type I ($\sim 10^{-1}$ 1/ns). Furthermore, for the type-I/II regime the rate is smaller by two more orders of magnitude (to $\sim 10^{-5}$ 1/ns). However, we note that in our CI calculations we omit the short-range interaction within the unit crystal cell. Thus we also neglect the effect of that on the emission rate, resulting in the difference to the experimental data. Moreover, we note that the data presented in Figs. 5(a) and 5(c) show unusual dips and peaks, in particular for Se contents of ~ 0.15 and 0.3 which is a result of the numerical errors present in our $\mathbf{k} \cdot \mathbf{p}$ +CI calculations in combination with the nature of the transition between different types of confinement, which might need more elaborate methods [61] for more precise description.

The aforementioned behavior can be understood with inspection of the probability densities given in Fig. 4. We see that in type I [Fig. 4(a)] both electron and hole probability densities reside inside the QD body; hence the overlap is the largest of the studied types of confinement. On the other hand, in type II [Fig. 4(b)] while the electrons still reside inside the QD, holes are pushed to the surrounding ZnTe material above and below QD, which also explains the reduced oscillator strength of X^0 . The confinement for holes is provided by the band-edge changes caused by the elastic strain around QD and piezoelectricity originating in lattice mismatch between dot and buffer materials [7,42]. Finally, for type I/II in Fig. 4(c), we find the holes to be confined again inside the QD body. However, the holes, in particular those lowest in energy, are

confined on the outskirts of QD and their overlap with electrons is very faint as the wave functions almost exactly “miss” each other. It is that kind of behavior, combining localization of holes inside QD with very small overlap with electrons, that led us to the nomenclature of this confinement as type I/II.

However, the aforementioned analysis of the radiative emission rate of X^0 from Cd(Se,Te)/ZnTe QDs indicates that both type II and type I/II regimes are very hard to be accessed by optical means, as the dots would emit one photon in $\sim 1 \mu\text{s}$ or even in $\sim 100 \mu\text{s}$ for the former and latter confinements, respectively.

Finally, we would like to comment on the topology of the hole wave functions in Cd(Se,Te)/ZnTe QDs. From the probability densities shown in Fig. 4, we can observe that the holes for type-II and type-I/II [Figs. 4(b) and 4(c)] have a toroidal shape for both ground and excited SP states. Thus the hole states in Cd(Se,Te)/ZnTe QDs with type II or type I/II might be utilized for the realization of the Aharonov-Bohm effect [70], similarly as was proposed, e.g., in Ref. [71].

V. CONCLUSIONS

We have studied the excitonic structure of Cd(Se,Te) QDs embedded in the ZnTe matrix. The PL spectroscopy analysis revealed a reduction of FSS of ground-state exciton with increasing Se content in dots. This was found to be associated with type-II character of the dots for larger Se contents. We

confirmed this by detailed $\mathbf{k} \cdot \mathbf{p}$ and CI calculations, the results of which explained the experimentally observed trends very well. The theory identified the main mechanism causing larger FSS, in particular in type-I dots, to be due to the multipole expansion of the exchange interaction. Furthermore, using our theory we found that for Se contents in the dot larger than ~ 0.3 a peculiar type I/II confinement occurs, causing an almost purely LH character of exciton and toroidal shape of hole states.

ACKNOWLEDGMENTS

P.W. acknowledges the financial supported from the National Centre of Science (Poland) through Grant No. 2017/26/E/ST3/00253. P.K. was financed by the project CUSPIDOR, which has received funding from the QuantERA ERA-NET Cofund in Quantum Technologies implemented within the European Union’s Horizon 2020 Programme. In addition, this project has received national funding from the Ministry of Education, Youth and Sports of the Czech Republic and funding from European Union’s Horizon 2020 (2014-2020) research and innovation framework programme under Grant Agreement No. 731473. The work reported in this paper also was partially funded by projects 20IND05 QADeT, 20FUN05 SEQUME, 17FUN06 SIQUST that received funding from the EMPIR programme cofinanced by the Participating States and from the European Union’s Horizon 2020 research and innovation programme.

- [1] I. Aharonovich, D. Englund, and M. Toth, Solid-state single-photon emitters, *Nat. Photonics* **10**, 631 (2016).
- [2] P. Senellart, G. Solomon, and A. White, High-performance semiconductor quantum-dot single-photon sources, *Nat. Nanotechnol.* **12**, 1026 (2017).
- [3] S. Thomas and P. Senellart, The race for the ideal single-photon source is on, *Nat. Nanotechnol.* **16**, 367 (2021).
- [4] N. Tamm, A. Javadi, N. O. Antoniadis, D. Najer, M. C. Löbl, A. R. Korsch, R. Schott, S. R. Valentin, A. D. Wieck, A. Ludwig, and R. J. Warburton, A bright and fast source of coherent single photons, *Nat. Nanotechnol.* **16**, 399 (2021).
- [5] A. Orioux, M. A. Versteegh, K. D. Jöns, and S. Ducci, Semiconductor devices for entangled photon pair generation: a review, *Rep. Prog. Phys.* **80**, 076001 (2017).
- [6] D. Huber, M. Reindl, J. Aberl, A. Rastelli, and R. Trotta, Semiconductor quantum dots as an ideal source of polarization-entangled photon pairs on-demand: A review, *J. Opt.* **20**, 73002 (2018).
- [7] P. Klenovský, V. Křápek, D. Munzar, and J. Humlíček, Modelling of electronic states in InAs/GaAs quantum dots with GaAsSb strain reducing overlayer, *J. Phys.: Conf. Series.* **245**, 012086 (2010).
- [8] P. Klenovský, D. Hemzal, P. Steindl, M. Zíková, V. Křápek, and J. Humlíček, Polarization anisotropy of the emission from type-II quantum dots, *Phys. Rev. B* **92**, 241302(R) (2015).
- [9] M. Müller, S. Bounouar, K. D. Jöns, M. Glässl, and P. Michler, On-demand generation of indistinguishable polarization-entangled photon pairs, *Nat. Photonics* **8**, 224 (2014).
- [10] S. Strauf, N. G. Stoltz, M. T. Rakher, L. A. Coldren, P. M. Petroff, and D. Bouwmeester, High-frequency single-photon source with polarization control, *Nat. Photonics* **1**, 704 (2007).
- [11] D. Huber, M. Reindl, S. F. Covre da Silva, C. Schimpf, J. Martín-Sánchez, H. Huang, G. Piredda, J. Edlinger, A. Rastelli, and R. Trotta, Strain-Tunable GaAs Quantum Dot: A nearly Dephasing-Free Source of Entangled Photon Pairs on Demand, *Phys. Rev. Lett.* **121**, 033902 (2018).
- [12] J. Liu, R. Su, Y. Wei, B. Yao, S. Filipe, Y. Yu, J. Iles-Smith, K. Srinivasan, A. Rastelli, J. Li, and X. Wang, A solid-state source of strongly entangled photon pairs with high brightness and indistinguishability, *Nat. Nanotechnol.* **14**, 586 (2019).
- [13] H. Huang, D. Csontosová, S. Manna, Y. Huo, R. Trotta, A. Rastelli, and P. Klenovský, Electric field induced tuning of electronic correlation in weakly confining quantum dots, *Phys. Rev. B* **104**, 165401 (2021).
- [14] F. Basso Basset, M. Valeri, E. Rocca, V. Muredda, D. Poderini, J. Neuwirth, N. Spagnolo, M. B. Rota, G. Carvacho, F. Sciarrino, and R. Trotta, Quantum key distribution with entangled photons generated on demand by a quantum dot, *Sci. Adv.* **7**, 1 (2021).
- [15] C. Schimpf, M. Reindl, D. Huber, B. Lehner, S. F. Covre da Silva, S. Manna, M. Vyvlecka, P. Walther, and A. Rastelli, Quantum cryptography with highly entangled photons from semiconductor quantum dots, *Sci. Adv.* **7**, abe8905 (2021).
- [16] R. M. Stevenson, R. J. Young, P. Atkinson, K. Cooper, D. A. Ritchie, and A. J. Shields, A semiconductor source of

- triggered entangled photon pairs, *Nature (London)* **439**, 179 (2006).
- [17] G. Burkard, D. Loss, and D. P. DiVincenzo, Coupled quantum dots as quantum gates, *Phys. Rev. B* **59**, 2070 (1999).
- [18] P. Klenovský, A. Schliwa, and D. Bimberg, Electronic states of (inga)(assb)/gaas/gap quantum dots, *Phys. Rev. B* **100**, 115424 (2019).
- [19] P. Klenovský, V. Křápek, and J. Humlíček, Type-II InAs/GaAsSb/GaAs quantum dots as artificial quantum dot molecules, *Acta Phys. Pol. A* **129**, A62-5 (2016).
- [20] V. Křápek, P. Klenovský, A. Rastelli, O. G. Schmidt, and D. Munzar, Quantum entanglement in lateral gaas/algaas quantum dot molecules, *J. Phys. Conf. Ser.* **245**, 012027 (2010).
- [21] A. Marent, T. Nowozin, M. Geller, and D. Bimberg, The qd-flash: a quantum dot-based memory device, *Semicond. Sci. Technol.* **26**, 014026 (2011).
- [22] A. Marent, M. Geller, and D. Bimberg, A novel nonvolatile memory based on self-organized quantum dots, *Microelectron. J.* **40**, 492 (2009).
- [23] D. Bimberg, A. Marent, T. Nowozin, and A. Schliwa, Antimony-based quantum dot memories, Proc. SPIE 7947, Quantum Dots and Nanostructures Synthesis, Characterization, and Modeling VIII, 79470L (2011).
- [24] A. Marent, M. Geller, A. Schliwa, D. Feise, K. Pötschke, D. Bimberg, N. Akçay, and N. Öncan, 10^6 years extrapolated hole storage time in gasb/alas quantum dots, *Appl. Phys. Lett.* **91**, 242109 (2007).
- [25] E. M. Sala, G. Stracke, S. Selve, T. Niermann, M. Lehmann, S. Schlichting, F. Nippert, G. Callsen, A. Strittmatter, and D. Bimberg, Growth and structure of in_{0.5}ga_{0.5}sb quantum dots on gap(001), *Appl. Phys. Lett.* **109**, 102102 (2016).
- [26] E. M. Sala, I. F. Arikan, L. Bonato, F. Bertram, P. Veit, J. Christen, A. Strittmatter, and D. Bimberg, Mowpe-growth of ingasb/alp/gap(001) quantum dots for nanoscale memory applications, *Phys. Status Solidi B* **255**, 1800182 (2018).
- [27] R. Trotta, E. Zallo, C. Ortix, P. Atkinson, J. D. Plumhof, J. van den Brink, A. Rastelli, and O. G. Schmidt, Universal Recovery of the Energy-Level Degeneracy of Bright Excitons in Ingaas Quantum Dots Without a Structure Symmetry, *Phys. Rev. Lett.* **109**, 147401 (2012).
- [28] R. Trotta, E. Zallo, E. Magerl, O. G. Schmidt, and A. Rastelli, Independent control of exciton and biexciton energies in single quantum dots via electroelastic fields, *Phys. Rev. B* **88**, 155312 (2013).
- [29] R. Trotta, J. Martín-Sánchez, J. S. Wildmann, G. Piredda, M. Reindl, C. Schimpf, E. Zallo, S. Stroj, J. Edlinger, and A. Rastelli, Wavelength-tunable sources of entangled photons interfaced with atomic vapours, *Nat. Commun.* **7**, 10375 (2016).
- [30] J. Martín-Sánchez, R. Trotta, A. Mariscal, R. Serna, G. Piredda, S. Stroj, J. Edlinger, C. Schimpf, J. Aberl, T. Lettner, J. Wildmann, H. Huang, X. Yuan, D. Ziss, J. Stangl, and A. Rastelli, Strain-tuning of the optical properties of semiconductor nanomaterials by integration onto piezoelectric actuators, *Semicond. Sci. Technol.* **33**, 013001 (2017).
- [31] J. Aberl, P. Klenovský, J. S. Wildmann, J. Martín-Sánchez, T. Fromherz, E. Zallo, J. Humlíček, A. Rastelli, and R. Trotta, Inversion of the exciton built-in dipole moment in in(ga)as quantum dots via nonlinear piezoelectric effect, *Phys. Rev. B* **96**, 045414 (2017).
- [32] P. Klenovský, P. Steindl, J. Aberl, E. Zallo, R. Trotta, A. Rastelli, and T. Fromherz, Effect of second-order piezoelectricity on the excitonic structure of stress-tuned in(ga)as/gaas quantum dots, *Phys. Rev. B* **97**, 245314 (2018).
- [33] M. C. Löbl, L. Zhai, J.-P. Jahn, J. Ritzmann, Y. Huo, A. D. Wieck, O. G. Schmidt, A. Ludwig, A. Rastelli, and R. J. Warburton, Correlations between optical properties and voronoi-cell area of quantum dots, *Phys. Rev. B* **100**, 155402 (2019).
- [34] D. Huber, B. U. Lehner, D. Csontosová, M. Reindl, S. Schuler, S. F. Covre da Silva, P. Klenovský, and A. Rastelli, Single-particle-picture breakdown in laterally weakly confining gaas quantum dots, *Phys. Rev. B* **100**, 235425 (2019).
- [35] D. Csontosová and P. Klenovský, Theory of magneto-optical properties of neutral and charged excitons in gaas/algaas quantum dots, *Phys. Rev. B* **102**, 125412 (2020).
- [36] A. Rastelli, S. Stuffer, A. Schliwa, R. Songmuang, C. Manzano, G. Costantini, K. Kern, A. Zrenner, D. Bimberg, and O. G. Schmidt, Hierarchical Self-Assembly of GaAs/AlGaAs Quantum Dots, *Phys. Rev. Lett.* **92**, 166104 (2004).
- [37] E. M. Sala, Y. I. Na, M. Godsland, A. Trapalis, and J. Heffernan, InAs/InP quantum dots in etched pits by droplet epitaxy in metalorganic vapor phase epitaxy, *Phys. Status Solidi Rapid Res. Lett.* **14**, 2000173 (2020).
- [38] K. Matsuda, S. V. Nair, H. E. Ruda, Y. Sugimoto, T. Saiki, and K. Yamaguchi, Two-exciton state in GaSb GaAs type II quantum dots studied using near-field photoluminescence spectroscopy, *Appl. Phys. Lett.* **90**, 013101 (2007).
- [39] J. M. Miloszewski, S. Tomić, and D. Binks, Theoretical studies of excitons in type II CdSe/CdTe quantum dots, *J. Phys.: Conf. Ser.* **526**, 012005 (2014).
- [40] M. Jo, M. Sato, S. Miyamura, H. Sasakura, H. Kumano, and S. I. Origin of the blueshift of photoluminescence in a type-ii heterostructure, *Nanoscale Res. Lett.* **7**, 654 (2012).
- [41] M. P. Young, C. S. Woodhead, J. Roberts, Y. J. Noori, M. T. Noble, A. Krier, E. P. Smakman, P. M. Koenraad, M. Hayne, and R. J. Young, Photoluminescence studies of individual and few GaSb/GaAs quantum rings, *AIP Adv.* **4**, 117127 (2014).
- [42] P. Klenovský, V. Křápek, D. Munzar, and J. Humlíček, Electronic structure of inas quantum dots with gaassb strain reducing layer: Localization of holes and its effect on the optical properties, *Appl. Phys. Lett.* **97**, 203107 (2010).
- [43] P. Klenovský, P. Steindl, and D. Geffroy, Excitonic structure and pumping power dependent emission blue-shift of type-ii quantum dots, *Sci. Rep.* **7**, 45568 (2017).
- [44] D. Mourad, J. P. Richters, L. Gérard, R. André, J. Bleuse, and H. Mariette, Determination of valence-band offset at cubic CdSe/ZnTe type-II heterojunctions: A combined experimental and theoretical approach, *Phys. Rev. B* **86**, 195308 (2012).
- [45] P. Wojnar, J. Płachta, A. Reszka, J. Lähnemann, A. Kaleta, S. Kret, P. Baranowski, M. Wójcik, B. J. Kowalski, L. T. Baczewski, G. Karczewski, and T. Wojtowicz, Near-infrared emission from spatially indirect excitons in type II ZnTe/CdSe/(Zn,Mg)Te core/double-shell nanowires, *Nanotechnology* **32**, 495202 (2021).
- [46] S. Kim, B. Fisher, H. J. Eisler, and M. Bawendi, Type-II quantum dots: CdTe/CdSe(core/shell) and CdSe/ZnTe(core/shell) heterostructures, *J. Am. Chem. Soc.* **125**, 11466 (2003).

- [47] F. Tinjod, B. Gilles, S. Moehl, K. Kheng, and H. Mariette, II-VI quantum dot formation induced by surface energy change of a strained layer, *Appl. Phys. Lett.* **82**, 4340 (2003).
- [48] P. Wojnar, C. Bougerol, E. Bellet-Amalric, L. Besombes, H. Mariette, and H. Boukari, Towards vertical coupling of CdTe/ZnTe quantum dots formed by a high temperature tellurium induced process, *J. Cryst. Growth* **335**, 28 (2011).
- [49] Y. Léger, L. Besombes, L. Maingault, and H. Mariette, Valence-band mixing in neutral, charged, and Mn-doped self-assembled quantum dots, *Phys. Rev. B* **76**, 045331 (2007).
- [50] T. Kazimierzczuk, T. Smoleński, M. Goryca, Ł. Kłopotowski, P. Wojnar, K. Fronc, A. Golnik, M. Nawrocki, J. A. Gaj, and P. Kossacki, Magnetophotoluminescence study of intershell exchange interaction in CdTe/ZnTe quantum dots, *Phys. Rev. B* **84**, 165319 (2011).
- [51] T. Smoleński, M. Koperski, M. Goryca, P. Wojnar, P. Kossacki, and T. Kazimierzczuk, Optical study of a doubly negatively charged exciton in a CdTe/ZnTe quantum dot containing a single Mn 2+ ion, *Phys. Rev. B* **92**, 085415 (2015).
- [52] T. Kazimierzczuk, M. Goryca, M. Koperski, A. Golnik, J. A. Gaj, M. Nawrocki, P. Wojnar, and P. Kossacki, Picosecond charge variation of quantum dots under pulsed excitation, *Phys. Rev. B* **81**, 155313 (2010).
- [53] E. Deleporte, J. M. Berroir, C. Delalande, N. Magnea, H. Mariette, J. Allegre, and J. Calatayud, Excitonic effects in separate-confinement quantum-well heterostructures CdTe/(Cd,Zn)Te, *Phys. Rev. B* **45**, 6305 (1992).
- [54] P. Baranowski, M. Szymura, G. Karczewski, M. Aleszkiewicz, A. Rodek, T. Kazimierzczuk, P. Kossacki, T. Wojtowicz, J. Kossut, and P. Wojnar, Optical signatures of type I-type II band alignment transition in Cd(Se,Te)/ZnTe self-assembled quantum dots, *Appl. Phys. Lett.* **117**, 113101 (2020).
- [55] K. Kowalik, O. Krebs, A. Golnik, J. Suffczyński, P. Wojnar, J. Kossut, J. A. Gaj, and P. Voisin, Manipulating the exciton fine structure of single CdTe ZnTe quantum dots by an in-plane magnetic field, *Phys. Rev. B* **75**, 195340 (2007).
- [56] V. Křápek, P. Klenovský, and T. Šikola, Excitonic fine structure splitting in type-II quantum dots, *Phys. Rev. B* **92**, 195430 (2015).
- [57] M. Ściesiek, J. Suffczyński, W. Pacuski, M. Parlińska-Wojtan, T. Smoleński, P. Kossacki, and A. Golnik, Effect of electron-hole separation on optical properties of individual Cd(Se,Te) quantum dots, *Phys. Rev. B* **93**, 195313 (2016).
- [58] K. Wei, F. H. Pollak, J. L. Freeouf, D. Shvydka, and A. D. Compaan, Optical properties of CdTe_{1-x}S_x (0<x<1): Experiment and modeling, *J. Appl. Phys.* **85**, 7418 (1999).
- [59] S. Birner, T. Zibold, T. Kubis, A. Sabathil, and P. Vogl, nextnano: General purpose 3-d simulations, *IEEE Trans. El. Dev.* **54**, 2137 (2007).
- [60] T. Zibold, Ph.D. thesis, Technische Universität München, 2007.
- [61] A. Mittelstädt, A. Schliwa, and P. Klenovský, Modeling electronic and optical properties of iii-v quantum dots—selected recent developments, *Light Sci. Appl.* **11**, 17 (2022).
- [62] A. Schliwa, M. Winkelkemper, and D. Bimberg, Few-particle energies versus geometry and composition of in_xga_{1-x}As/GaAs self-organized quantum dots, *Phys. Rev. B* **79**, 075443 (2009).
- [63] P. A. M. Dirac, The quantum theory of the emission and absorption of radiation, *Proc. R. Soc. A* **114**, 243 (1927).
- [64] O. Stier, Ph.D. thesis, Technische Universität Berlin, 2000.
- [65] T. Takagahara, Theory of exciton doublet structures and polarization relaxation in single quantum dots, *Phys. Rev. B* **62**, 16840 (2000).
- [66] P. Klenovsky, J. Valdhans, L. Krejčí, M. Valtr, P. Klapetek, and O. Fedotova, Interplay between multipole expansion of exchange interaction and Coulomb correlation of exciton in colloidal II-VI quantum dots, *Electron. Struct.* **4**, 015006 (2022).
- [67] R. Vrijen and E. Yablonovitch, A spin-coherent semiconductor photo-detector for quantum communication, *Phys. E* **10**, 569 (2001).
- [68] Y. H. Huo, B. J. Witek, S. Kumar, J. R. Cardenas, J. X. Zhang, N. Akopian, R. Singh, E. Zallo, R. Grifone, D. Kriegner, R. Trotta, F. Ding, J. Stangl, V. Zwiller, G. Bester, A. Rastelli, and O. G. Schmidt, A light-hole exciton in a quantum dot, *Nat. Phys.* **10**, 46 (2014).
- [69] V. Křápek, P. Klenovský, and T. Šikola, Type-i and type-ii confinement in quantum dots: Excitonic fine structure, *Acta Phys. Pol. A* **129**, A66 (2016).
- [70] Y. Aharonov and D. Bohm, Significance of electromagnetic potentials in the quantum theory, *Phys. Rev.* **115**, 485 (1959).
- [71] J. M. Llorens, V. Lopes-Oliveira, V. López-Richard, E. R. Cardozo de Oliveira, L. Wewiór, J. M. Ulloa, M. D. Teodoro, G. E. Marques, A. García-Cristóbal, G.-Q. Hai, and B. Alén, Topology Driven *g*-Factor Tuning in Type-II Quantum Dots, *Phys. Rev. Applied* **11**, 044011 (2019).